Renewable and Sustainable Energy Reviews 52 (2015) 1527–1538

Contents lists available at ScienceDirect

Renewable and Sustainable Energy Reviews

journal homepage: www.elsevier.com/locate/rser

Overview of high-efficiency organic photovoltaic materials and devices

Xuxu Liu, Huajie Chen, Songting Tan *

College of Chemistry, and Key Laboratory of Environmentally Friendly Chemistry and Applications of Ministry of Education, Xiangtan University, Xiangtan 411105, China

ARTICLE INFO

Article history:
Received 14 November 2014
Received in revised form
25 May 2015
Accepted 10 August 2015

Key words:
Bulk-heterojunction
Organic solar cells
Photovoltaic materials
Photovoltaic devices

ABSTRACT

Organic solar cells based on conjugated polymers or small molecules are a promising alternative to silicon-based solar cells due to the potential advantages in fabricating low-cost, light-weight, and flexible devices. Recently, great advances have been made in the development of high-efficiency photovoltaic materials and device structures. The highest power conversion efficiency has exceeded 11%. In this review, we focus on donor–acceptor polymers and small molecules for high-efficiency solar cells, and summarize the most recent developments in the optimization of device engineering. The analysis about the structure–property relationship may guide the rational design and evaluation of photovoltaic materials and device structures.

1. Introduction

Bulk-heterojunction organic solar cells (BHJ-OSCs) have attracted widespread attention from chemical, physical and material scientists [1,2]. The "bulk-heterojunction", where the active layer comprises a blend of bicontinuous and interpenetrating electron donor and acceptor components in a bulk volume, is sandwiched between transparent indium tin oxide (ITO) glass and a metal electrode. Nowadays two kinds of active layer materials, π-conjugated polymers and small molecules, are used as electron donor materials in BHJ-OSCs. These π-conjugated polymers and small molecules are key components in the development of solution-processed OSCs. Compared to the conventional inorganic silicon-based materials, these organic photovoltaic materials have unique advantages such as low cost, light-weight, solution-processed over large-area substrates, and flexibility, etc. [3,4].

In more than a decade, following the development of BHJ architecture, the unremitting efforts of numerous researchers have led to the yearly growing power conversion efficiencies (PCEs), which is demonstrated in Fig. 1. Before 2009, the PCEs grew relatively slow, with almost no large promotions. However, after 2009, with the sharp increase of researches in BHJ-OSCs, PCEs are being lifted to a new height each year, which indicates the promising future in BHJ-OSCs. Here, this review is divided into two main aspects, high-efficiency active layer materials including electron donor and acceptor materials, as well as the development of organic photovoltaic devices.

2. High-efficiency active layer materials

2.1. Electron donor materials

2.1.1. Conjugated polymers

As a consequence of improved photovoltaic performances of materials, the use of conjugated polymers as electron donor materials has recently obtained an exciting growth in interest as the PCEs of polymer solar cells (PSCs) have increased over the past few years [5]. To cover the state-of-art developments, we summarize recent studies on a selection of high-performance polymers in PSCs, and the corresponding characteristics are summarized in Table 1. These polymer photovoltaic materials have attracted much attention from the scientific community because of their promising results.

Thiophene is a very important and popular heterocyclic compound to construct conjugated polymer donors for high-efficiency PSCs. Among all the thiophene derivatives, poly-3-hexylthiophene (P3HT, Fig. 2), is the most typical one. It has not only excellent solubility and high hole mobility, but also good crystallinity, which is attributed to the well-defined molecular structure [6,7]. But its high-lying energy level of highest occupied molecular orbital (HOMO) goes against high open-circuit voltage (V_{oc}) and broad absorption spectrum, which limits its development. As a result, significant progress has been achieved in developing new

* Corresponding author. Tel.: +86 731 58292251.
E-mail address: tanst2008@163.com (S. Tan).

http://dx.doi.org/10.1016/j.rser.2015.08.032
1364-0321/

Abbreviations

Nomenclature

BHJ	bulk-heterojunction
SMBHJ	small molecule bulk-heterojunction
OSCs	organic solar cells
PSCs	polymer solar cells
ITO	transparent indium tin oxide
HOMO	highest occupied molecular orbital
LUMO	lowest occupied molecular orbital
PCEs	power conversion efficiencies
V_{oc}	open-circuit voltage
J_{sc}	short-circuit current density
FF	fill factor
D	donor
A	acceptor
P3HT	poly-3-hexylthiophene
$PC_{71}BM$	[6,6]-phenyl-C71-butyric acid methyl ester
$PC_{61}BM$	[6,6]-phenyl-C61-butyric acid methyl ester
ICBA	Indene – C60 bisadduct
HTL	hole transport layer
ETL	electron transport layer
PEDOT:PSS	poly(3,4-ethylenedioxythiophene):poly (styrenesulfonate)
TT	thieno[3,4-b]thiophene
BDT	benzodithiophene
BDTP	benzodithiophene alkylthienyl
PTB	poly(2,5-mothieno[3,4-b]thiophene dialkoxyl benzodithiophene)
BDTT	thienylbenzodithiophene
DTBT	4,7-di(thien-2-yl)-2,1,3-benzothiadiazole
DPP	diketopyrrolopyrrole
DTS	dithienosilole
DTG	dithienogermole
TIPD	titanium (diisopropoxide) bis(2,4-pentanedionate)
UVO	ultraviolet–ozone
PFN	poly [(9,9-bis(3-(*N*,*N*-dimethylamino) propyl)-2,7-fluorene)-*alt*-2,7-(9,9-dioctylfluorene)]
ID	isoindigo
DTC	dithieno[3,2-*b*;6,7-*b*]carbazole
EQE	external quantum efficiency
ICL	interconnection layer
IPCE	incident photon-to-electron conversion efficiency
R2R	roll-to-roll
LCOE	levelized cost of energy
EPBT	energy payback time

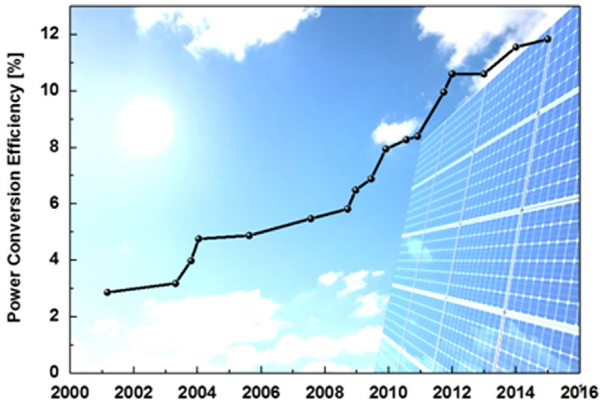

Fig. 1. Yearly growing PCEs in BHJ-OSCs.

active-layer polymer photovoltaic materials by the structure optimization of P3HT.

Since 2009, Yu et al. had developed a series of novel polymers (PTB) based on alternating ester substituted thieno[3,4-b]thiophene (TT) and benzodithiophene (BDT) units [8]. The rigid backbone of these polymers led to the good hole mobility. The stabilization of quinoidal structure from TT resulted in a low band gap of about 1.6 eV, and the introduction of fluorine into TT provided the polymer with a relatively deep HOMO energy level, which offered an enhanced V_{oc}. After an extensive structural optimization, they further developed a new polymer from the PTB family, PTB7, namely P1a in Fig. 2. A high PCE of 7.4% was achieved from P1a and [6,6]-phenyl-C_{71}-butyric acid methyl ester ($PC_{71}BM$) based solar cell device, which was the first PSC showing a PCE over 7% [9]. Recently, Li et al. introduced an alkylthio

Table 1
Characteristics of BHJ-OSCs based on the polymers as electron donors.

Electron donors	Electron acceptors	E_{LUMO} (eV)	E_{HOMO} (eV)	E_g^{opt} (eV)	μ_h ($cm^2\ V^{-1}\ s^{-1}$)	V_{oc} (V)	J_{sc} (mA cm^{-2})	FF (%)	PCE (%)	Ref.
P1a	$PC_{71}BM$	−3.31	−5.15	1.68	5.8×10^{-4}	0.74	14.5	69	7.40	[9]
P1b	$PC_{71}BM$	−3.17	−5.30	1.58	2.8×10^{-3}	0.78	15.4	61	7.40	[10]
P1b	$PC_{71}BM$	−3.74	−5.49	1.59	8.0×10^{-4}	0.79	19.8	65	10.12	[12]
P1c	$PC_{71}BM$	−3.27	−5.41	1.57	4.1×10^{-3}	0.84	15.3	65	8.42	[10]
P1d	$PC_{71}BM$	−3.52	−5.33	1.51	1.0×10^{-2}	0.80	17.5	68	9.48	[11]
P2	$PC_{71}BM$					0.97	12.6	70	8.50	[13]
P3b	$PC_{71}BM$		−5.22	1.68	3.0×10^{-3}	0.82	15.6	64	8.20	[15]
P4b	$PC_{71}BM$	−3.40	−5.10	1.40	5.2×10^{-2}	0.61	18.6	64	7.30	[16]
P4c	$PC_{71}BM$	−3.50	−5.10	1.40	6.6×10^{-2}	0.60	18.7	62	6.90	[16]
P5a	$PC_{71}BM$		−5.35	1.70	8.9×10^{-2}	0.88	12.9	71	8.07	[18]
P5b	$PC_{61}BM$	−3.20	−5.31	1.70	3.7×10^{-2}	0.78	15.4	69	8.30	[22]
P6	$PC_{71}BM$	−3.30	−5.52	1.73	2.3×10^{-3}	0.76	18.2	58	8.00	[23]
P7c	$PC_{71}BM$	−3.70	−5.25	1.38	6.9×10^{-4}	0.69	16.8	62	7.20	[25]
P8	$PC_{61}BM$	−3.80	−5.37	1.57	8.9×10^{-5}	0.72	16.2	64	7.25	[26]
P9a	$PC_{71}BM$	−3.73	−5.55	1.82	5.9×10^{-2}	0.80	12.5	80	7.90	[27]
P9b	$PC_{71}BM$	−3.77	−5.58	1.81	2.8×10^{-3}	0.86	12.9	78	8.66	[27]
P10	$PC_{71}BM$	−3.69	−5.45	1.76	3.0×10^{-3}	0.79	16.3	73	9.39	[28]
P11a	$PC_{71}BM$	−3.88	−5.57	1.73	1.0×10^{-4}	0.88	12.2	68	7.30	[29]
P11b	$PC_{71}BM$			1.70		0.86	15.2	65	8.20	[30]
P12	$PC_{71}BM$	−3.73	n.a.	1.43		0.75	15.9	67	8.00	[31]

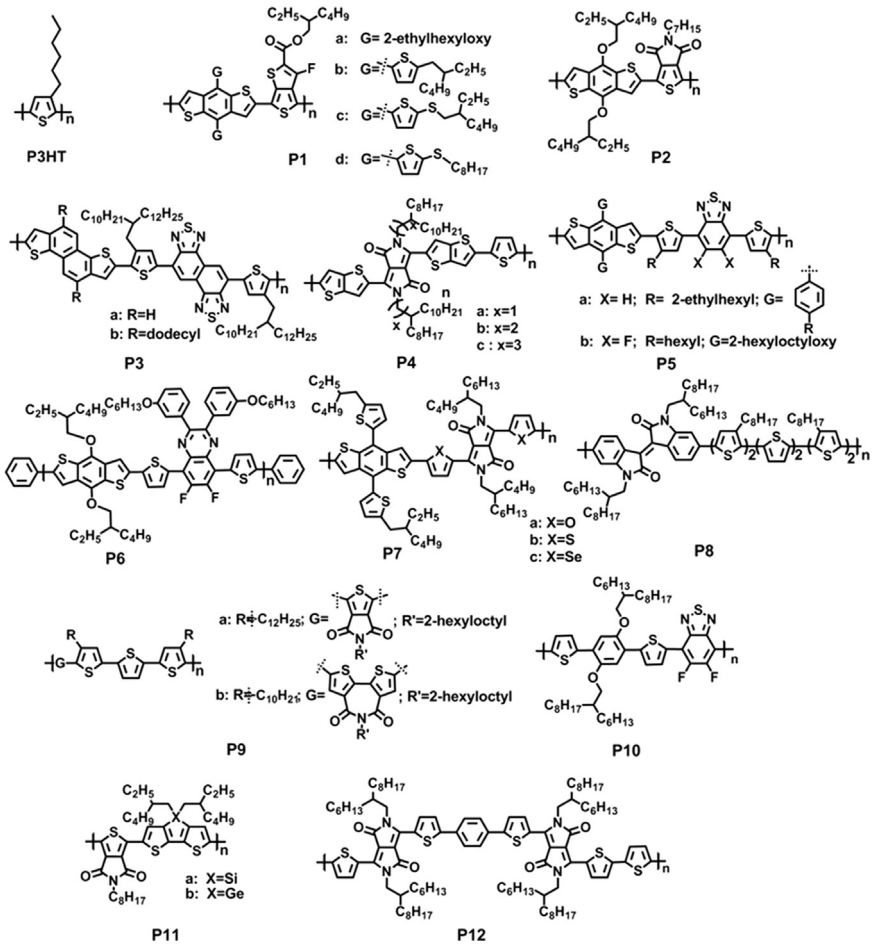

Fig. 2. Chemical structures of P3HT and copolymers P1–P12.

substituent to the thiophene side chain of BDT unit and synthesized a new low-band-gap polymer P1c (Fig. 2) [10]. As is commonly known, the electron-donating ability of sulfur is weaker than oxygen, and sulfur atom has some π-acceptor capability. Therefore, compared with P1b (Fig. 2), the alkylthio substituent on BDT unit of P1c slightly red-shifted the absorption band in the polymer film and down-shifted the HOMO energy level of the polymer, which benefited the V_{oc}. Consequently, the PSC based on P1c:$PC_{71}BM$ exhibited a high V_{oc} of 0.84 V, leading to a high PCE of 8.42%, while the V_{oc} and PCE of the P1b-based device under the optimized fabrication conditions were 0.77 V and 7.42%, respectively. Subsequently, by replacing 2-ethylhexyl with *n*-octyl group on the BDT side chain, Hou's group designed and synthesized a novel two-dimensional conjugated polymer P1d (Fig. 2) and the PSC device based on P1d obtained a high PCE up to 9.48% [11]. Very recently, with a sequence of optimization, especially for the BHJ layer thickness, Gong et al. pushed the PCE of P1b-based PSC device up to 10.12% with a significant enhancement in J_{sc} value [12], indicating the importance of optimization for active layer thickness in PSC devices.

Beaujuge et al. investigated the self-assembling properties of polymer and found that the linear side-chain substitutions in polymers could greatly impact the PCEs in PSCs [13]. The switching of branched side-chains by linear ones on the BDT unit caused a great change in polymer self-assembling properties and backbone orientation in thin films, leading to a dramatic decrease in the PCEs of BHJ devices. On the other hand, in the polymers with branched alkyl-substituted BDT units, controlling the number of aliphatic carbons in linear *N*-alkyl-substituted thienopyrrole-4,6-dione (TPD) motifs did not significantly affect preferential backbone orientation, but it could be a key in improving the photovoltaic performance. Thus, *N*-heptyl-substituted TPD-based polymer P2 (Fig. 2) got a PCE of 8.5% and a V_{oc} of 0.97 V in a conventional BHJ device with $PC_{71}BM$, which was a significant improvement when compared to their *N*-octyl-substituted counterparts (7.5%). In 2012, Takimiya et al. demonstrated that the introduction of linear alkyl chains also brought about a critical change in polymer orientation, which was beneficial for the charge transport in PSCs. They reported a new polymer P3a (Fig. 2), comprising naphtho-[1,2-*b*:5,6-*b*′]dithiophene (NDT3) and naphtho[1,2-*c*:5,6-*c*′]-bis[1,2,5]thiadiazole (NTz). But due to its poor solubility, the P3a-based PSC device only obtained a PCE of 4.9% [14]. After that, they introduced linear alkyl groups to the 5,10-positions of NDT3 unit, the polymers showed an excellent improvement in solubility. Besides, a key change in the orientation from edge-on to face-on was accompanied by the alkylation, without an alteration of the energy levels, resulting in a quite high PCE of 8.2% for a conventional single-junction solar cell based on P3b and $PC_{71}BM$ [15].

Systematically moving the alkyl-chain branching position away from the backbone of P4a afforded two new polymers P4b and P4c (Fig. 2) based on TT and diketopyrrolopyrrole (DPP), which was reported by Meager et al. [16]. This was the first time that the location of the branching point had been shown to influence the orientation of the conjugated backbone plane and improve the crystallinity of the polymers. When P4b and P4c were used as donor materials in PSCs, PCEs of 7.3% and 6.9% were achieved, respectively.

To tune the structural and electronic properties of polymers, a new monomer (BDTP) with an alkylphenyl group attached to the

BDT unit instead of the alkylthienyl group was developed by Yang and his coworkers [17]. They found that BDTP-based polymers exhibited similar photovoltaic performances and relatively higher V_{oc} in comparison with thienylbenzodithiophene (BDTT)-based polymers. Afterwards, Hou et al. copolymerized the BDTP unit with 4,7-di(thien-2-yl)-2,1,3-benzothiadiazole (DTBT), generating a new polymer P5a (Fig. 2). The PSCs based on P5a and $PC_{71}BM$ showed a PCE of 8.07% with a V_{oc} of 0.88 V, a short-circuit current density (J_{sc}) of 12.94 mA cm^{-2}, and a fill factor (FF) of 0.71 [18]. As is well-known, inserting high electron-affinity fluorine atoms on acceptor units can further lower the HOMO and LUMO energy levels of polymers to attain higher V_{oc} [19]. Consequently, 4,7-di (thien-2-yl)-5,6-difluoro-2,1,3-benzothiadiazole (DTBTff), as an electron withdrawing unit, has attracted much attention in PSCs [20,21]. Based on the DTBTff unit, Chen et al. successfully synthesized a new conjugated polymer P5b (Fig. 2) through the change of different side chains. A PCE of 8.30% was achieved for P5b-based PSC device. Excellent photoelectric properties and good solubility affirmed P5b as a promising donor material for high-performance PSCs [22]. Afterwards, a special fluorinated quinoxaline-based conjugated polymer P6 (Fig. 2) was designed and synthesized by Chou et al. [23]. Based on the intrachain D–A copolymer motif, the polymer exhibited a broad and strong absorption spectrum. The introduction of F atom to the quinoxaline moiety gave P6 a high V_{oc} of 0.76 V. With a high J_{sc} of 18.2 mA cm^{-2}, and FF of 0.58, a high PCE of 8.0% was obtained.

Altering the atom on an acceptor unit sometimes can also improve the device performance. In 2012, Yang et al. demonstrated a series of polymers based on alternating DPP and BDTT units [17]. When the BDTT unit was copolymerized with the furan-containing DPP unit (FDPP), the resulting polymer P7a (Fig. 2) gave a low PCE in a single-junction solar cell. By switching the furan to a thiophene moiety, P7b (Fig. 2) showed an increased J_{sc} and FF, resulting in a higher PCE of 6.5% [24]. Subsequently, they discovered a selenium-substituted low-band-gap polymer P7c (Fig. 2) [25]. The substitution of O or S by Se atom on the DPP unit brought about an enhanced hole mobility and a reduced band gap for the polymers. A high PCE of 7.2% was obtained in the P7c-based PSC device, which was a significant enhancement compared to its counterparts P7a and P7b.

By increasing the length of thiophene unit, the absorption spectrum can be broadened, and the polymer displays better crystallinity and hole mobility, while the HOMO and LUMO energy levels remain within suitable range for PSCs. Recently, a series of isoindigo-based polymers with extended thiophene units in the polymer main chains were synthesized by Su et al. [26]. The polymer P8 (Fig. 2) gained a high J_{sc} of 16.24 mA cm^{-2} and the highest PCE of 7.25% among all the reported isoindigo-based copolymers up to now.

Although PSC mechanisms are affected by many factors, highly-ordered microstructures with close π–π interplanar spacings, vertical D–A phase gradation and ordered BHJ bicontinuous networks can also contribute to the superior charge carrier mobility, which in turn results in a high FF and PCE. Recently, Marks et al. reported two new polymers P9a and P9b (Fig. 2) [27]. They exhibited high PCEs of 7.9% and 8.7%, respectively, principally caused by the increased V_{oc} and exceptional FF of 0.76–0.80. In 2014, Nguyen et al. reported a series of high-efficiency semi-crystalline photovoltaic polymers with noncovalent conformational locking to enhance chain planarity, intermolecular ordering and thermal stability, leading to highly ordered film morphologies, balanced electron and hole mobility, as well as exceptional device stability [28]. The thick active layer of 290 nm in the P10 (Fig. 2): $PC_{71}BM$ device enabled strong light absorption, yielding a high J_{sc} without the loss in V_{oc} and FF. Thus, the PSC device based on P10 obtained a high PCE of 9.39% for single-junction PSCs.

The copolymers based on dithienosilole (DTS) and dithienogermole (DTG) possess broad band gap, deep-lying HOMO energy level, strong chain interactions, and superior charge transport capability, which have attracted extensive attention in the BHJ-OSCs. In 2011, Tao et al. [29] reported a new polymer P11a (Fig. 2) comprising DTS and TPD units, with a deep HOMO energy level and a low optical band gap. The polymer solubility was improved via the introduction of branched alkyl chains to the DTS unit. The device based on P11a exhibited a PCE of 7.3%. In 2013, So et al. demonstrated the loss mechanism in thick-film solar cells based on P11b (Fig. 2) and got a high PCE of 8.2% for the device with an active layer thickness (L) of 204 nm [30]. While for $L > 200$ nm, the cell performance could not be maintained due to a reduction of FF, which was attributed to the limited charge collection efficiency caused by the space-charge accumulation.

In addition to the binary polymers, ternary polymers have been a new favorite in the BHJ-OSCs in recent years. A regular D1–A–D2–A or D–A1–D–A2 alternating terpolymer [32–38] exhibits superior performance, including high molecular weight, refined absorption range, and energy level control, when compared to the corresponding D–A binary polymers. Furthermore, the regular D1–A–D2–A alternation allows quantification of the exact chemical composition, and reduces local variations in HOMO and LUMO energy levels which can reduce charge carrier mobility and broaden the state density [39]. Recently, Janssen's group developed a new terpolymer P12 by using DPP as the electron-deficient unit, combined with electron-rich terthiophene and thiophene–phenylene–thiophene moieties. Because of the fine-tuned energy levels and optical band gap, the PSC based on terpolymer P12 showed a PCE up to 8.0% [31].

2.1.2. Small molecules

As a competitive alternative to the conjugated polymers counterpart, solution-processed small molecule based BHJ (SMBHJ) solar cells have attracted considerable attention in the last decades, due to their potential advantages in terms of easy purification, well-defined and versatile molecular structure, definite molecular weight, less batch-to-batch variations, and amenability to large-scale production. A great variety of SMBHJ materials have been reported recently, indicating that some techniques for PSCs can also be applied to SMBHJs [40–42]. It has been revealed that the absorption characteristics, energy levels, charge carrier mobility, and even photoelectric properties can be controlled via the careful design of small molecules. Recently, small molecular donors have been developed, and donor–acceptor (D–A) small molecules attached with soluble substituents are now being systematically studied as a more promising candidate for BHJ-OSC application [43]. The chemical structures of small molecules with high efficiencies and the characteristics of BHJ-OSCs based on the small molecules as electron donors are showed in Fig. 3 and Table 2, respectively.

The first recorded PCE over 7% in SMBHJ solar cells was reported by Chen and his team [44]. Considering the relatively large planar structure and low HOMO energy level of BDT, two A–D–A type small molecules M1a and M1b (Fig. 3) with BDT as the central donor and octylcyanoacetate and 3-ethylrhodanine as different terminal acceptors were synthesized, respectively. The device based on M1b with 3-ethylrhodanine terminal unit owned a much higher J_{sc} than that of the octylcyanoacetate terminated M1a, because 3-ethylrhodanine significantly improved solar light absorption. So the M1b-based SMBHJ solar cell obtained a PCE of 7.38%. Afterwards, they developed two small molecules, M1c and M1d (Fig. 3) by introducing the thiophene units to the BDT moiety, resulting in larger conjugation and red shift in the solution UV–vis spectra of M1c when compared to M1b. The PCEs of 8.12% and

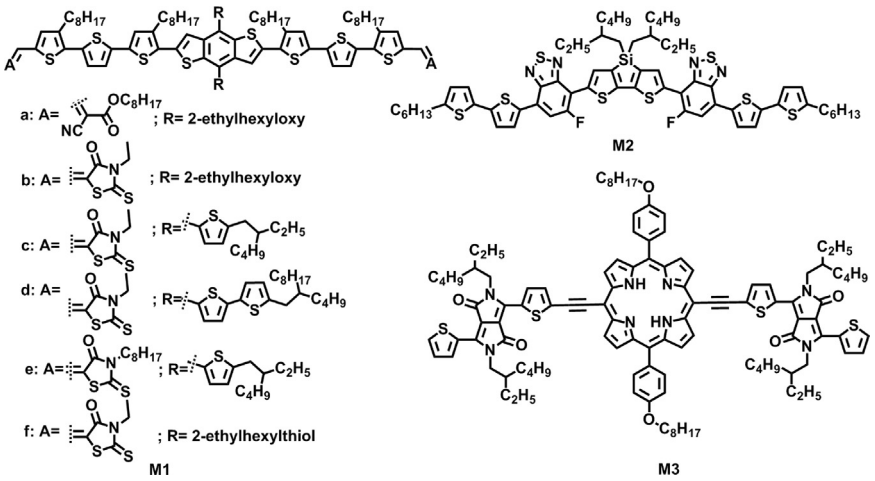

Fig. 3. Chemical structures of small molecules M1–M3.

Table 2
Characteristics of BHJ-OSCs based on the small molecules as electron donors.

Electron donors	Electron acceptors	E_{LUMO} (eV)	E_{HOMO} (eV)	E_g^{opt} (eV)	μ_h ($cm^2 V^{-1} s^{-1}$)	V_{oc} (V)	J_{sc} (mA cm^{-2})	FF (%)	PCE (%)	Ref.
M1b	$PC_{71}BM$	−3.27	−5.02	1.74	2.47×10^{-4}	0.93	12.2	65	7.38	[44]
M1c	$PC_{71}BM$	−3.27	−5.02	1.72	2.88×10^{-4}	0.93	13.2	66	8.12	[45]
M1d	$PC_{71}BM$	−3.29	−5.07	1.76	3.29×10^{-4}	0.92	12.1	72	8.02	[45]
M1e	$PC_{71}BM$	−3.60	−5.50	1.90	3.3×10^{-4}	0.94	12.2	70	8.02	[46]
M1f	$PC_{71}BM$	−3.30	−5.07	1.74	6.13×10^{-4}	0.92	14.6	74	9.95	[47]
M2	$PC_{71}BM$	−3.34	−5.12	1.55		0.81	12.8	68	7.00	[48]
M2	$PC_{71}BM$	−3.34	−5.12	1.55		0.77	14.7	72	8.24	[49]
M3	$PC_{61}BM$	−3.60	−5.07	1.36	4.68×10^{-4}	0.71	16.0	64	7.23	[50]

8.02% were achieved for M1c- and M1d-based SMBHJ solar cells, respectively [45]. Later on, Yang's group designed and synthesized a new conjugated small molecule M1e (Fig. 3), which was similar to M1c, while they changed 3-ethylrodanine to 3-octylrodanine as the electron-withdrawing terminal acceptor. The long linear alkyl chains on 3-octylrodanine terminal unit improved the solubility and film quality of M1e. The single-junction solar cell based on M1e exhibited a remarkable PCE of 8.02% [46]. In 2014, Chen's group reported a new small molecule M1f (Fig. 3), which possessed a similar chemical structure compared with M1a except for the replacement of oxygen with a sulfur atom in the BDT side chain [47]. With thermal annealing and solvent vapor annealing, a notable PCE of 9.95% was achieved for M1f-based device, which is one of the highest PCE for single-junction SMBHJ solar cells. The striking result was attributed to the significant improvement of J_{sc} and FF, which was originated from the enhanced absorption, preferable morphology, as well as the higher and more balanced charge motility.

Similar to the studies of BDT-modified systems, small molecules with DTS units as the central building blocks have also been developed recently. Bazan et al. synthesized a fluorinated DTS-based small molecule M2 in Fig. 3 [48]. The M2-based PSC device gave a PCE of 7.0% with a V_{oc} of 0.81 V, a J_{sc} of 12.8 mA cm^{-2}, and a FF of 0.68. Afterwards, Heeger et al. improved the PCE of M2-based PSC up to 8.24% by using a low sheet resistance of ITO (5 Ω/□) substrate, due to an increased J_{sc} of 14.7 mA cm^{-2} and FF of 0.72, which originated from the reduced series resistance (Rs) [49].

Porphyrin is a kind of macromolecular heterocyclic compound, which is formed by alpha carbon atoms with four pyrrole subunits interconnected via the methine bridges. It is a planar and highly conjugated 26-π-electrons system. Porphyrin derivatives have been widely used in BHJ-OSCs due to their large π-conjugation systems, superior photochemical and thermal stabilities. Porphyrin derivatives also offer flexibility in their optical and electronic properties through synthetic modifications. Recently, a small molecule M3 (Fig. 3) with two symmetric diketopyrrolopyrrole (DPP) units in porphyrin periphery was designed and synthesized by Peng's group [50]. The compound containing porphyrin core exhibited good charge-transporting ability and enhanced π–π stacking in its solid film. The cell based on M3 exhibited a PCE up to 7.23%, which is the highest PCE based on porphyrins and their derivatives in conventional SMBHJs up to now.

In view of the aforementioned versatile structures, there is still great room for designing more favorable small molecules for high-efficiency solar cells through delicate molecule designs and device optimizations. With higher PCEs for SMBHJ solar cells, the landmark value required for possible commercialization can be achieved in the near future.

2.2. Electron acceptor materials

In the rapid development of BHJ-OSCs, electron acceptors are of the same importance as the electron donors. The compatibility of donor and acceptor material exerts a tremendous influence on the micro-morphology of the active layer, while the matching condition of energy level determines whether the carrier can separate effectively. However, research efforts devoted to the electron acceptors are much less than electron donors in BHJ-OSCs. Although carbon nanotubes, condensed ring compound, and some inorganic semiconductor nanoparticles etc. were used as electron acceptors through trial and error [51], but their performances are lower than fullerenes and their derivatives. Thus, the fullerenes and their derivatives are still the most widely used electron acceptors, wherein C_{60} and C_{70} are the typical ones.

C_{60} contains an extensively conjugated three-dimensional system consisting of 60 π-electrons, resulting in a strong reducibility, and it can absorb up to six electrons. Furthermore, C_{60} has a high electron affinity, low LUMO energy level and good electron-transporting

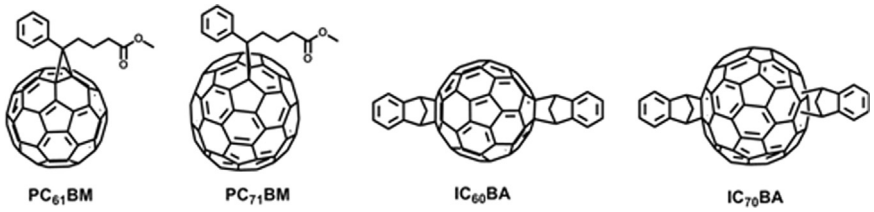

Fig. 4. Chemical structures of some fullerene derivatives.

properties. Meanwhile, another fullerene, named C_{70}, possesses 70 π-electrons and exhibits a wider absorption spectrum than C_{60}. These characteristics make C_{60} and C_{70} be promising electron acceptors in BHJ-OSCs [52–55]. However, the unmodified C_{60} and C_{70} have poor solubility and film-forming properties, and it can easily self-assemble, therefore they must be modified to be applied in BHJ-OSCs. Generally, some methods of stem grafting have been adopted to increase the solubility, where $PC_{61}BM$ and $PC_{71}BM$ (Fig. 4) are the most popular ones. $PC_{61}BM$ was first reported in PSC applications in 1995 [1,56], and since then better acceptors have scarcely been found. $PC_{61}BM$ possesses good solubility, low LUMO energy level (−3.91 eV), and relatively high electron mobility (10^{-3} cm^2 V^{-1} s^{-1}). However, due to the high degree of symmetry of C_{60}, $PC_{61}BM$ has relatively poor absorption in the visible region. To overcome that, Janssen and co-workers synthesized a new C_{70} derivative $PC_{71}BM$ with strong absorption in 400–500 nm [57]. Moreover, $PC_{71}BM$ possesses the same high electron mobility and better solubility compared to $PC_{61}BM$, which draws much attention of researchers. However, $PC_{71}BM$ is costly, which greatly limits its practical application.

In 2010, a new C_{60} derivative, Indene−C60 bisadduct (ICBA, Fig. 4), which can be easily obtained from the hot trichlorobenzene solution of indene, was developed by Li and his team [58]. It has better solubility than $PC_{61}BM$ in common solvents and a strong absorption in the range of 300–500 nm, which is very favorable for the absorption spectrum of OSCs. The devices based on the P3HT: ICBA have high V_{oc} and PCEs due to the relatively high LUMO energy level of ICBA (0.17 eV higher than $PC_{61}BM$), which is more capable of matching the energy level of P3HT. Thus, these properties of ICBA have caught the attention of researchers and made it be extensively applied in BHJ-OSCs, especially in tandem cells.

3. Development of organic photovoltaic devices

The BHJ-OSC research mainly concentrates on enhancing PCE and improving stability and operation life of solar cells. To realize that, the promotion and perfection of preeminent photovoltaic devices such as optimization of active layer morphology, interface modification, and improved device architectures are also critical apart from high-efficiency photovoltaic materials. Up to now, the optimization of active layer morphology has been a routine in enhancing the PCEs. In this section, we mainly discuss the interface modification and device architectures.

3.1. Device stability

Except for the high efficiency, the long-term stability of OSC devices has been recognized to be essential for the research in academia and industry [59]. Inorganic silicon-based solar cells may last on the order of 25 years, so the stability of OSC devices must be improved tremendously toward the wide success and commercialization [60]. After the first questions asked by a technological representative from industry which were: how efficient is it, how stable is it, what is the cost and what is the required investment in infrastructure, the attempt to answer these questions has resulted in a large amount of reports on stability with this industrial view in mind [61–66].

Generally, OSCs are complicated multilayer structures where each component may fail for different reasons and layers may even interact chemically and physically in ways that may cause degradation [67]. To sum up, physical and/or chemical degradation modes of OSC devices can be divided in two main categories: one is the intrinsic degradation due to changes in the characteristics of the interface between layers caused by internal modification of the materials, the other one is the extrinsic degradation owing to the changes in the cell behavior induced by external triggers, such as water, oxygen, electromagnetic radiations (UV, visible light, IR, etc.) [62].

OSCs suffer from degradation processes brought about by reaction of the materials with oxygen or moisture, and this can be prevented by encapsulation of the active layer in polymeric, inorganic or hybrid barrier coatings. Often the simplest way is covering the active layer with glass, and in this case, edge sealing is the most important problem [68]. In 2012, Tanenbaum et al. explored the seal around the edges of roll-to-roll processed devices and found that edge sealing could impart significant stability even though the adaptability to product integration was lost [69]. At present, the roll-to-roll (R2R) fabrication process is a feasible way to realize the large-scale production and commercial application of OSCs, and the fast and efficient encapsulation in the R2R fabrication can be easily put in force.

In conventional structure, the low-work-function metal is susceptible to degradation by oxygen and moisture, so the new concept of inverted structure and low-work-function interfacial materials were introduced into OSCs to improve the long-term stability. Besides, the hole transport layer (HTL), poly(3,4-ethylenedioxythiophene): poly(styrenesulfonate) (PEDOT:PSS), is acidic and corrosive to the ITO electrode, causing the stability problems in the OSCs. Therefore, new high-work-function interfacial materials have been developed [70]. This section will be divided into two parts and discussed in detail later.

Additionally, the micro-phase-separation, developed through the process of annealing, is very important to obtain efficient and stable devices [67]. Nowadays, promising approaches to address morphological instabilities of BHJ devices involve facilitating the photo-crosslinking of active layer and enhancing the glass transition temperature (T_g). In 2015, McCulloch's group utilized a small molecule crosslinker bis-azide 1,6-diazidohexane (DAZH) in devices, which allows the phase morphology to be 'locked' affording thermally stable blends with suppressed fullerene acceptor crystallization, thus increased the thermal stability and the PCE of as-cast devices (from 6% to 7%) [71]. Recently, Kesters et al. found that the stability of the photovoltaic cells under prolonged thermal stress was enhanced by the insertion of ester or alcohol moieties on the CPDT side chains, which could be attributed to the suppressed reorganization of the active layer components resulted from high T_g of the PCPDTBT-type copolymers [72].

Nowadays, the field of OSCs undergoes a rapid development where most of the research efforts have been placed on developing devices with an improved efficiency, while the equally important area of enhancing the device stability that has received less

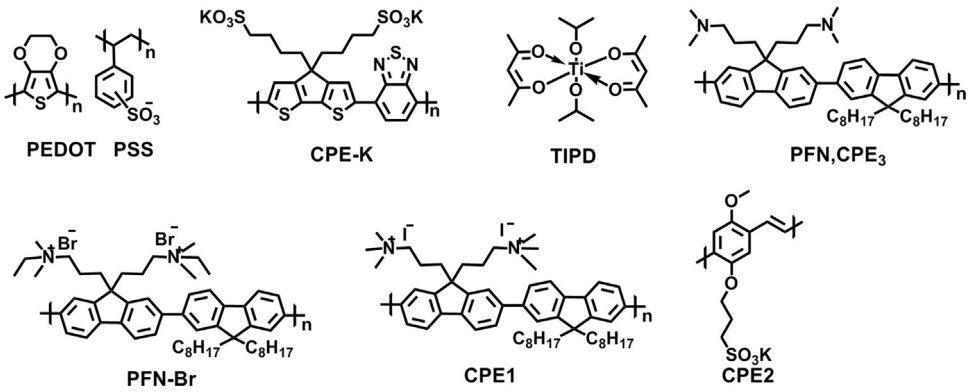

Fig. 5. Chemical structures of interfacial materials.

attention. But one can safely anticipate that along with the further improvement of PCEs in devices, the device stability will be the next research hotspot.

3.2. Interface modification

In order to improve the collection efficiency of carrier, and reduce the potential barrier on the interface, a HTL and an electron transport layer (ETL) are generally introduced into the device architectures of BHJ-OSCs. Usually, a HTL, between the active layer and anode, is a high-work-function material. It can effectively resist the injection of electrons, and also plays a role in transporting holes. In a conventional device structure, a HTL is disposed on the anode, which requires good transparency, so PEDOT:PSS (Fig. 5) is a preferred HTL material. PEDOT:PSS can act as a part in smoothing the rough electrode surface and increasing the work function of electrode. Additionally, it is able to strengthen the internal electric-field in devices, and enhance hole-extracting rate and hole mobility, leading to the improved PCEs of devices [73]. Though PEDOT:PSS has an appreciable improvement in photovoltaic performances of BHJ-OSCs, its acidic nature etches the ITO glass and increases potential instability on device lifetimes [74]. Therefore, a number of transition metal oxides (MoO_3, V_2O_5, NiO, ReO_x, and WO_3, etc.) with high transparency and environmental stability as well as moderate conductivity have been developed to modify the anode interface for efficient and stable OSCs [75–82].

Recently, Tan et al. demonstrated several solar cell devices modified by highly transparent solution-processed rhenium oxide (s-ReO_x) HTL [83]. The device based on P3HT:$IC_{60}BA$ exhibited a PCE of 7.26%, which is the highest value reported so far for the P3HT:$IC_{60}BA$ based PSCs. Moreover, the PCE of PSC based on the polymer poly(4,8-bis(5-(2-ethylhexyl)-thiophene-2-yl)-benzo[1,2-*b*:4,5-*b*′]dithiophene-*alt*-alkylcarbonyl-thieno[3,4-b]thiophene) (PBDTTT-C-T) and $PC_{71}BM$ with s-ReO_x as the HTL was improved to 8.30%, which was increased by 14% compared to that of PSC devices with PEDOT:PSS as the HTL. The improved PCE could be ascribed to the effective hole-extracting property of s-ReO_x layer and the enhanced absorption in the range of 400–550 nm. Heeger's group reported a water/alcohol soluble conjugated polyelectrolyte, PCPDTBT–SO_3–K (CPE-K, Fig. 5), which could be used as a HTL in organic photoelectric devices [84]. The CPE-K HTL exhibited great advantages over PEDOT:PSS, including a more homogeneous interface, a reduced Rs, and pH neutral nature. So the P1a-based PSC with the CPE-K HTL exhibited a high PCE of 8.2%.

The ETL between the active layer and cathode can effectively block the injection of holes and it also contributes to electron transport. A low-work-function metal, metal oxide, metal chelate or organic material can be used as an ETL material. In a conventional device structure, an ETL is placed on the active layer, and the transparency is not necessary.

Usually, Al is the most common cathode material, and other low work function metals such as Ca, Mg and Ba can be employed as the ETLs to protect the fragile organic films from damage, while being capped by the Al electrode [85,86]. Other inorganic materials, including LiF, CsF, Cs_2CO_3, CsCl, and BCP (bathocuproine) are also popular ETLs in BHJ-OSCs. Transparent semiconducting metal oxide such as TiO_2 can also be employed as the ETL because of its processability and non-toxicity [87–89]. The TiO_2 layer is an effective diffusion barrier against oxygen and water due to its scavenging effects, originating from photocatalysis and oxygen deficiency [87,90]. By incorporating the TiO_x layer, Heeger et al. demonstrated relatively air-stable PSCs with enhanced photovoltaic performances in 2007 [91]. The TiO_x layer prevented the intrusion of oxygen and humidity into the active polymers, thereby improving the lifetime of unsealed devices exposed to air by nearly two orders of magnitude. Among all the above mentioned inorganic materials, LiF and Ca are the most successful ETLs in OSCs.

Except for the inorganic materials, more and more polar organic materials have also been successfully applied as the ETLs in BHJ-OSCs. In contrast to n-type inorganic semiconductors, the organic materials can be easily solution-processed. Nowadays, different ETL materials have been widely applied in inverted and tandem cells and they will be discussed in detail afterwards.

3.3. Inverted structure

In BHJ-OSCs, the active layer and cathode affect the stability of the conventional devices. Particularly, the cathode is susceptible to degradation by oxygen and water. Generally, PEDOT:PSS is often employed as a HTL in conventional PSCs. However, long-term stability is a great challenge because PEDOT:PSS is acidic and hygroscopic [67,74,92–94]. In order to overcome these problems, the inverted structure for OSCs has been developed. For inverted OSC devices, air-stable high-work-function metals are used as the anode to collect holes, and ITO is used as the cathode to collect electrons. Considering that the ETL is placed on ITO electrode, a transparent material must be chosen. N-type metal oxides such as TiO_x, ZnO, and Cs_2CO_3 are deposited onto the ITO electrode to break the symmetry [95–97]. The elimination of acid PEDOT:PSS layer can significantly improve the device stability. Moreover, in an inverted structure, a high-work-function metal was used as an anode, which can be readily fabricated by solution coating or printing technology to lower the manufacturing cost [98]. Some amazing achievements have been made in inverted BHJ-OSCs.

Incorporating deterministic aperiodic nanostructures (DANs) based on nano-imprint technology on P1b:$PC_{71}BM$ device for

broad and self-enhanced light absorption with optimum charge extraction, Li et al. demonstrated a high-performance inverted single-junction PSC with a PCE of 10.1%, which is one of the most efficient single-junction PSC devices reported to date [99]. Compared with the reference device fabricated with a flat structure [100], the patterned device achieved an enhanced light harvesting, leading to an increase by 18% in photocurrent without sacrificing the charge transport properties.

In 2011, So et al. reported an effective method for enhancing charge collection in inverted solar cells by using a ultraviolet–ozone (UVO) treated ZnO-poly(vinyl pyrrolidone) (PVP) nanocomposite film as the ETL [101]. The UVO treatment to ZnO NP films could effectively reduce the defects caused by interface recombination, leading to a reduction in photocurrent loss and in turn an increase in PCEs of the inverted PSCs [102]. Thus, a high PCE of 8.5% was demonstrated for the inverted BHJ solar cell based on P11b (Fig. 2). Besides, the inverted PSC device with a UVO-treated ZnO-PVP nanocomposite ETL exhibited a much better stability. Notably, in 2013, Adhikary et al. reported a PBDTTT-C-T/$PC_{71}BM$ PSC device, and its ETL was subjected to UVO treatment, pushing the efficiency from 6.46% to 8.34% [103].

Wu et al. successfully demonstrated a high-performance inverted PSC based on P1a (Fig. 2), in which an alcohol-soluble conjugated polymer, poly [(9,9-bis(3-(*N*,*N*-dimethylamino) propyl)-2,7-fluorene)-*alt*-2,7-(9,9-dioctylfluorene)] (PFN, Fig. 5), was used as the ETL to tune the work function of ITO [104]. The experimental absorbed incident photon flux density in the active layer of inverted device was increased by 10% compared to the conventional device. Thus, the inverted PSC gained a remarkably improved J_{sc} of over 17 mA cm^{-2}, resulting in a superior PCE of 9.2% and better ambient stability. Subsequently, Gong et al. fabricated an inverted BHJ PSC with a thin conjugated polyelectrolyte PFN–Br (Fig. 5) as the ETL to engineer the ZnO electron extraction layer and obtained a PCE of 8.4%, which was higher than that (6.1%) of the inverted one without the PFN–Br interfacial layer [105]. The PFN–Br interfacial layer ensured the excellent contact and interface adhesion between ZnO electron-extracting layer and the BHJ active layer, leading to an enhanced charge-transporting ability via suppressing bimolecular recombination.

Adopting a kind of titanium chelate, titanium (diisopropoxide) bis(2,4-pentanedionate) (TIPD, Fig. 5), as the ETL and air-stable MoO_3 as the HTL, Tan et al. fabricated an inverted PSC with poly (4,8-bis-alkyloxybenzo(1,2-*b*:4,5-*b*′)dithiophene-2,6-diyl-*alt*-(alkylthieno(3,4-*b*)thiophene-2-carboxylate)-2,6-diyl) (PBDTTT-C) and $PC_{71}BM$. The PCE of the inverted PSC with TIPD as ETL reached 7.4%, which was higher than that (6.4%) of the conventional device, due to the hydrophobic surface and the suitable electronic energy level of the TIPD layer [106].

In 2013, Geng et al. reported several conjugated polymers containing isoindigo (ID) derivatives and dithieno[3,2-b;6,7-b] carbazole (DTC). Among them, the PSC based on the conjugated polymer poly[*N*-dedocyldithieno[3,2-b;6,7-b]carbazole-*alt*-*N*,*N*′-di (2-octyldodecanyl)-isoindigo] P(IID-DTC) demonstrated the PCEs of 7.2% for the conventional device and 8.2% for the inverted device, respectively, using MoO_3 as a HTL and ZnO as an ETL [107]. The increased PCE was derived from the higher J_{sc} and FF, which might be attributed to an improved interfacial contact and a more efficient charge collection and less electron–hole recombination.

In 2013, Liao et al. introduced the fullerene derivative-doped ZnO nanofilm as an ETL, fabricating a sequence of PSC devices based on P1a or P1b (Fig. 2) [100]. And the inverted device based on P1b:$PC_{71}BM$ got a best PCE of 9.35% with ZnO–C60 ETL. Afterwards, they modified the ZnO ETL by dual doping with the novel fullerene derivative BisNPC60–OH and indium ($InCl_3$) simultaneously, and the device with the active layer P1b:$PC_{71}BM$ gave a PCE up to 10.31% [108], which is one of the best results that have been reported so far for single-junction PSCs.

Very recently, Nielsen et al. introduced a series of new versatile polymers, BBTI family, which consisted of a dithienyl flanked 2,1,3-benzothiadiazole-5,6-dicarboxylic imide (BTI) monomer and a benzo[1,2-*b*:3,4-*b*′:5,6-*d*′]trithiophene (BTT) unit, having ideal frontier energy levels for PSCs [109]. Thus, all of the polymers exhibited excellent miscibility with $PC_{71}BM$ acceptor without any additives or thermal or solvent-assisted annealing. Consequently, the inverted PSC device based on BBTI-1:$PC_{71}BM$ got the best efficiency of 8.3%. Afterwards, Zhang et al. presented an inverted PSC device based on a silole copolymer PSiNO containing ladder-type heptacylic arene and napthobisoxadiazole moieties, affording a remarkable PCE of 8.37% with a high V_{oc} of 0.90 V and FF of 0.70 [110].

3.4. Tandem structure

Although single-junction BHJ-OSCs have displayed impressive progress, it is not sufficient for commercial applications. Several groups have predicted that the PCE limitation of single-junction OSCs would be around 15%, through the optimization of materials with appropriate band gaps, energy levels, and charge-carrier mobility [111–113]. To achieve a higher PCE, a balanced consideration of J_{sc}, V_{oc}, and FF needs to be implemented. For example, to obtain a large J_{sc}, the development of low band gap materials has been demonstrated to be one of the most effective approaches. However, this method generally causes a decrease in V_{oc}. The limitations of single-junction photovoltaic devices can be overcome by using tandem or multi-junction solar cells, in which two or more single cells are stacked together with the complementary wavelength ranges [114–118]. Thus, the photon utilization efficiency can be significantly improved and thermalization losses can be lowered through the employment of materials with different band gaps, then the PCEs of BHJ-OSCs can be improved further.

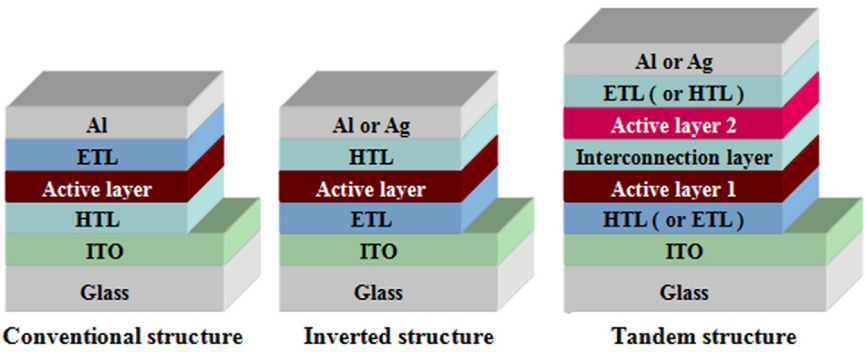

Fig. 6. Device architectures of conventional, inverted, and tandem cells.

Furthermore, recent more accurate models have predicted that the maximum efficiencies will be over 20% for this configuration [119,120]. Up to now, the reported non-single photovoltaic devices are mostly tandem architectures, so we mainly discuss the tandem devices with high performances in this section. The typical tandem structure is shown in Fig. 6.

In 2012, Yang and his team demonstrated a high-efficiency tandem PSC with P3HT:$IC_{60}BA$ as the front cell and PBDTT–DPP:$PC_{71}BM$ as the rear cell [24]. The front cell showed a strong absorption from 300 to 600 nm and external quantum efficiency (EQE) value up to 60% at 530 nm, while the rear cell showed the broad absorption band between 300 and 850 nm and a maximum EQE of 47% at 770 nm. So the inverted tandem PSC obtained a J_{sc} of 8.26 mA cm^{-2}. With a high V_{oc} of 1.56 V, which was the sum of two sub-cells, a high PCE of 8.62% was achieved. Subsequently, Yang's group reported a series of tandem PSCs based on PBDTT–DPP derivatives by copolymerizing BDTP or BDTT with DPP or furan-flanked DPP (FDPP) unit [17]. Because of the deeper HOMO levels and better charge-transporting properties of these low-band-gap polymers, the tandem PSCs showed the enhanced V_{oc}, J_{sc}, and FF values. All of the tandem devices showed a V_{oc} of about 1.6 V, which was equal to the addition of the front and rear cells, and the PBDTT–DPP, PBDTP–DPP, and PBDTT–FDPP based tandem devices achieved high PCEs of 8.8%, 8.5%, and 8.3%, respectively. In 2013, their team employed a poly[2,7-(5,5-bis-(3,7-dimethyloctyl)-5H-dithieno[3,2-*b*:2′,3′-*d*]pyran)-*alt*-4,7-(5,6-difluoro-2,1,3-benzothiadiazole)] (PDTP–DFBT) in the tandem solar cells for more efficient light harvesting. The absorption of the PDTP–DFBT:$PC_{71}BM$ based tandem cell was significantly improved when compared to the single-junction cells, especially in the visible region. As a result, the PCE was raised from 8.1% in single-junction cell to 10.2% in tandem cell [121]. Afterwards, to fine tune the balance of J_{sc}, different acceptor materials ($PC_{61}BM$ and $PC_{71}BM$) were used for the sub-cell by the same group [122]. For the tandem cell with $PC_{61}BM$, the integrated J_{sc} of the front and rear cell were both 9.8 mA cm^{-2}. While replacing $PC_{61}BM$ with $PC_{71}BM$, less photons from the metal electrode was absorbed by the front cell, due to the strong absorption of $PC_{71}BM$ in the visible region. Accordingly, the EQE value of the front cell at 300–600 nm was reduced, while that of the rear cell was increased. Finally, the integrated J_{sc} of the front cell was 9.5 mA cm^{-2}, while that of the rear cell was 10 mA cm^{-2}. As is well-known, the current of tandem solar cells is usually determined by the sub-cell with the lowest J_{sc}. Therefore, although the tandem cell with $PC_{71}BM$ showed an excellent FF of 0.69 and V_{oc} of 1.51 V, it presented a lower J_{sc} of 9.8 mA cm^{-2}. So it obtained a PCE of 10.2%, while the tandem cell with $PC_{61}BM$ got a higher PCE of 10.6%, with a higher J_{sc} of 10.1 mA cm^{-2}. The results demonstrated that the photovoltaic performances of tandem solar cells could be well-tuned by choosing different fullerene derivatives to adjust current matching.

In 2013, Peng et al. reported two novel D–A conjugated polymers PBDTFBZO and PBDTFBZS based on dialkylthiol substituted BDT and mono-fluorinated benzotriazole acceptor moieties. With the improved V_{oc}, J_{sc} and FF, a PCE of 7.74% was achieved in the single-junction device based on PBDTFBZS, while the PBDTFBZS-based tandem PSC showed a promising PCE up to 9.4% [123].

Jen et al. developed a tandem solar cell consisting of a front cell with P3HT:$IC_{60}BA$ and a rear cell with poly[2,6-(4,4-bis(2-ethylhexyl)-4H-cyclopenta[2,1-*b*;3,4-*b*′]dithiophene)-*alt*-4,7-(5-fluoro-2,1,3-benzothia-diazole)] (PCPDTFBT):$PC_{71}BM$ [124]. The two sub-cells were linked via an interconnection layer (ICL) comprising modified-PEDOT:PSS/high conductivity PEDOT:PSS (PH1000)/ZnO films. This ICL possessed a high optical transparency of about 85% at 700–900 nm, a reasonable conductivity, and a smooth surface. Consequently, the tandem cell showed a high PCE of 8.2% with a J_{sc} of 7.83 mA cm^{-2}, a V_{oc} of 1.57 V, and a FF of 0.67. The incident photon-to-electron conversion efficiency (IPCE) spectrum exhibited a broad spectral response range from UV to the near-IR region, which demonstrated that two sub-cells in the tandem cell work individually.

Tandem solar cells comprising two identical photoactive layers as sub-cells based on small molecule M1e (Fig. 3) were presented by Liu et al. in 2013 [46]. The device structure was ITO/PEDOT:PSS/M1e:$PC_{71}BM$/CPE1/CPE2/M-PEDOT:PSS/M1e:$PC_{71}BM$/CPE3/Al. And the chemical structures of the conjugated polyelectrolytes CPE1, CPE2, and CPE3 are shown in Fig. 5. The CPE bilayer formed an efficient pathway for electron transport and created an internal polarization field to lower the electron injection barrier from the front sub-cell to the middle ICL. The CPE-based ICL could be considered as Ohmic contact with a negligible resistance, leading to a notable FF of 0.72. Because of an obvious enhancement in V_{oc}, the tandem solar cell achieved a PCE of 10.1%, while the single-junction device was 8.1%. The EQE value in tandem device was 30% higher than that in single-junction device. But the internal quantum efficiency (IQE) values in single-junction and tandem devices were similar, indicating that the charge-extracting ability in tandem cell was as efficient as it was in the single-junction cell. While in 2015, based on the optimization of P1b:$PC_{71}BM$ single-junction cells, Heeger's group systematically investigated the effects of different HTLs as ICLs on the tandem structures [125]. The optimized tandem cell with ZnO/CPEPh–Na ICL achieved a best PCE of 11.3%, approximately a 25% enhancement in efficiency compared to the single-junction cells (9%). This enhancement arises primarily from the near total light harvesting.

Janssen et al. reported high-efficiency tandem solar cells based on the polymer PMDPP3T with the absorption region approaching 960 nm [126]. The tandem and triple junction PSCs based on PMDPP3T exhibited the high PCEs of 8.9% and 9.6%, respectively, which were much higher than that (6.0%) of the single-junction solar cells due to the highly complementary absorption layers in tandem and triple junction PSCs. Compared with the double-junction tandem cell, the triple-junction one showed a higher PCE, due to the exploitation of the excess current generation of the non-limiting sub-cell. Moreover, the remarkable increase in V_{oc} of the triple junction device (2.09 V vs. 1.49 V) compensated the loss in J_{sc}. The results confirmed that the triple-junction architecture can be a new useful method to improve the performance of tandem solar cell devices with unbalanced sub-cells.

As mentioned above, in some cases, triple-junction devices can minimally improve the performance of tandem cells. However, they are very difficult and costly to be implemented. The enhancement obtained in terms of efficiency does not always compensate these two issues and one has to carefully analyze whether this approach is worthy taking into account a potential mass production [120]. In any case, if only considering efficiency issues, the triple junction tandem cell could be worth trying in the exploration way for more efficient OSCs. In 2014, Forrest et al. used two relatively thick and strongly absorbing, vacuum-deposited small molecule planar mixed heterojunction sub-cells with considerable separation between their absorption maxima, thereby minimizing spectral overlap and maximizing photocurrent [127]. A primarily orange-to-near infrared (NIR) absorbing donor, 2-((7-(5-(dip-tolylamino)thiophen-2-yl)benzo[*c*][1,2,5]thiadiazol-4-yl) methylene) malononitrile (DTDCTB), blended with C_{60}, was applied as the front cell, paired with an UV-to-yellow absorbing DBP:C_{70} back sub-cell. The double-junction tandem solar cell exhibited a high PCE of 10.0%. Further improvements were demonstrated in the triple-junction architecture, when NIR was sandwiched between the absorbing donors and a second DBP:C_{70} sub-cell is placed as the middle sub-cell. They also recorded the astonishing enhancements in device performance, registering a high V_{oc} of 2.58 V, a J_{sc} of 7.3 mA cm^{-2}, and a high PCE of 11.1%.

In 2014, three complementary materials with different band gaps from 1.4 to 1.9 eV were used as electron donors to obtain balanced photon absorption rates and matched photocurrents among the sub-cells, Yang et al. demonstrated an efficient triple-junction tandem PSC with the PCE up to 11.55% [128]. Similarly, Yusoff et al. reported a series of highly efficient inverted double-junction and triple-junction devices, by making full use of band gap engineering [129]. The double-junction tandem architecture consisted of a wide-band-gap front sub-cell, poly[(4,4′-bis(3-ethylhexyl)-dithieno[3,2-*b*′′:3′-*d*]silole)-2,6-diyl-*alt*-(2,5-(3-(2-ethylhexyl)thiophen-2-yl)thiazolo[5,4-d]thiazole] (PSEHTT):$IC_{60}BA$, and a medium-band-gap bottom sub-cell, PTB7:$PC_{71}BM$. To further boost the efficiency, an additional low-band-gap third sub-cell, PMDPP3T:$PC_{71}BM$, was stacked to form an inverted triple-junction PSC. By using this technique, the inverted triple-junction PSC broadly covered the absorption wavelength from 300 to 800 nm in the solar spectrum, achieving a record-high PCE of 11.83%, along with a V_{oc} of 2.24 V, a FF of 0.68, and a J_{sc} of 7.83 mA cm^{-2}, suggesting huge potential for multi-junction PSCs research.

4. Summary and outlook

In this review, we have introduced some outstanding high-efficiency materials with promising components as well as optimized devices with different structures for BHJ-OSCs. On the whole, the advancement of record-high PCEs is driven by the development of novel electron donor and acceptor materials, implementation of innovative interfacial materials, application of different device structures, enhancement of device stability, and adoption of revolutionary processing conditions all this time. So far, many researchers have paid a great deal of attention to the research and development of BHJ-OSCs, leading to a breakthrough of about 12% in PCE, bringing a bright future for this exciting research field. Though impressive, the efficiency of BHJ-OSCs is still significantly lower than their inorganic counterparts, such as silicon, CdTe and CIGS, which prevents the practical applications on a large scale. Therefore, further improvement is required to modify the molecular structure of active materials and to optimize the device fabrication. The strategies on the design for organic photovoltaic materials and devices are summarized as follows:

On one hand, the strategies for high-performance organic photovoltaic materials can be to (1) attach proper alkyl (branching) chains as side chain or move the alkyl-chain position away from the backbone for improving the solubility of donor materials and adjusting the miscibility with the fullerene acceptor; (2) rationally construct new donor or acceptor units such as heterocyclic or multiring large π-conjugated structure for increasing the crystallinity and hole mobility of electron donor materials; (3) adjust the broad absorption spectra coupled with a high extinction coefficient of active layer for enhancing the J_{sc}; (4) well-match HOMO and LUMO energy levels between the donors and acceptors, as well as substitute a specific functional group or atom, such as ester, ketone, imide or fluorine for lowering the HOMO energy level and achieving a higher V_{oc}; (5) develop highly ordered, closely packed and properly oriented active-layer microstructures with optimal horizontal phase separation and vertical phase gradation for getting a higher FF; and (6) replace the binary polymerization with ternary polymerization at times for obtaining high molecular weight, refined absorption range and energy level control.

On the other hand, methods for highly efficient devices can be to (1) use the conventional ways for improving the morphology of active layer; (2) optimize interfacial materials for enhancing charge extracting rate and lowering the energy barrier; (3) adopt different electron acceptors for harvesting more absorption photons and matching the energy level; (4) engineer the device architectures applied in BHJ-OSCs such as inverted and tandem structures for enhancing the device performance; and (5) employ the triple junction tandem cell instead of the double junction one for getting a higher V_{oc} and a broader absorption.

Besides, there are many other improvements that need to be made towards the wide scale manufacture of OSCs such as improving device lifetime and lowering the cost of devices. While laboratory scale devices have recently been made with efficiencies over 10% in the single-junction architecture and over 11% with a multi-junction approach, there remains a significant drop in PCE on the module scale. Consequently, there is a significant need to improve module efficiencies, including identifying ways to translate lab scale performance to R2R processing and designing large-area modules that are able to reduce electrical losses. And the stability of these devices will also need to be improved in parallel [130].

The challenges for the next level of optimization in BHJ-OSCs have been delineated here, and focus not only on cementing a much deeper level of physical understanding of the involved means, but developing and optimizing new processes to capitalize on such new knowledge. The pursuit of such optimizations promises to be an informative and ultimately useful endeavor. A greater understanding of the interactions at the interfaces of a given cell architecture, and the improvements at both the novel material and device architecture levels of water and oxygen stability will raise efficiency up to 15% or even higher and push the low-cost BHJ-OSCs to final commercialization. Encouragingly, key economic indicators suggest that OSCs will become competitive with traditional energy sources as a result of a low levelized cost of energy (LCOE) and outstanding energy payback time (EPBT) due to their lightweight and high-throughput, R2R solution processing, and the rapid progress of this field instills continued confidence in this technology. In a word, there is a lot more work to be done but the prospect of BHJ-OSCs is splendid and worth the efforts.

Acknowledgments

This work was supported by the National Natural Science Foundation of China (51173154, 21474081, 51403177), and Hunan Provincial Natural Science Foundation of China (13JJ2025).

References

[1] Yu G, Gao J, Hummelen JC, Wudl F, Heeger AJ. Polymer photovoltaic cells: enhanced efficiencies via a network of internal donor–acceptor heterojunctions. Science 1995;270:1789–90.
[2] Günes S, Neugebauer H, Sariciftci NS. Conjugated polymer-based organic solar cells. Chem Rev 2007;107:1324–38.
[3] Lin Y, Li Y, Zhan X. Small molecule semiconductors for high-efficiency organic photovoltaics. Chem Soc Rev 2012;41:4245–72.
[4] Beaujuge PM, Fréchet JMJ. Molecular design and ordering effects in π-functional materials for transistor and solar cell applications. J Am Chem Soc 2011;133:20009–29.
[5] Duan C, Huang F, Cao Y. Recent development of push–pull conjugated polymers for bulk-heterojunction photovoltaics: rational design and fine tailoring of molecular structures. J Mater Chem 2012;22:10416–34.
[6] Street RA. Conducting polymers: the benefit of order. Nat Mater 2006;5:171–2.
[7] Kline RJ, McGehee MD, Toney MF. Highly oriented crystals at the buried interface in polythiophene thin-film transistors. Nat Mater 2006;5:222–8.
[8] Liang Y, Feng D, Wu Y, Tsai S, Li G, Ray C, et al. Highly efficient solar cell polymers developed via fine-tuning of structural and electronic properties. J Am Chem Soc 2009;131:7792–9.
[9] Liang Y, Xu Z, Xia J, Tsai S, Wu Y, Li G, et al. For the bright future—bulk heterojunction polymer solar cells with power conversion efficiency of 7.4%. Adv Mater 2010;22:135–8.
[10] Cui C, Wong W, Li Y. Improvement of open-circuit voltage and photovoltaic properties of 2D-conjugated polymers by alkylthio substitution. Energy Environ Sci 2014;7:2276–84.
[11] Ye L, Zhang S, Zhao W, Yao H, Hou J. Highly efficient 2D-conjugated benzodithiophene-based photovoltaic polymer with linear alkylthio side chain. Chem Mater 2014;26:3603–5.

[12] Liu C, Yi C, Wang K, Yang Y, Bhatta RS, Tsige M, et al. Single-junction polymer solar cells with over 10% efficiency by a novel two-dimensional donor–acceptor conjugated copolymer. ACS Appl Mater Interfaces 2015;7:4928–35.
[13] Cabanetos C, El Labban A, Bartelt JA, Douglas JD, Mateker WR, Fréchet JM, et al. Linear side chains in benzo [1, 2-b: 4, 5-b′] dithiophene—thieno [3, 4-c] pyrrole-4, 6-dione polymers direct self-assembly and solar cell performance. J Am Chem Soc 2013;135:4656–9.
[14] Osaka I, Abe T, Shimawaki M, Koganezawa T, Takimiya K. Naphthodithiophene-based donor–acceptor polymers: versatile semiconductors for OFETs and OPVs. ACS Macro Lett. 2012;1:437–40.
[15] Osaka I, Kakara T, Takemura N, Koganezawa T, Takimiya K. Naphthodithiophene – naphthobisthiadiazole copolymers for solar cells: alkylation drives the polymer backbone flat and promotes efficiency. J Am Chem Soc 2013;135:8834–7.
[16] Meager I, Ashraf RS, Mollinger S, Schroeder BC, Bronstein H, Beatrup D, et al. Photocurrent enhancement from diketopyrrolopyrrole polymer solar cells through alkyl-chain branching point manipulation. J Am Chem Soc 2013;135:11537–40.
[17] Dou L, Gao J, Richard E, You J, Chen C, Cha KC, et al. Systematic investigation of benzodithiophene- and diketopyrrolopyrrole-based low-bandgap polymers designed for single junction and tandem polymer solar cells. J Am Chem Soc 2012;134:10071–9.
[18] Zhang M, Gu Y, Guo X, Liu F, Zhang S, Huo L, et al. Efficient polymer solar cells based on benzothiadiazole and alkylphenyl substituted benzodithiophene with a power conversion efficiency over 8%. Adv Mater 2013;25:4944–9.
[19] Stuart AC, Tumbleston JR, Zhou H, Li W, Liu S, Ade H, et al. Fluorine substituents reduce charge recombination and drive structure and morphology development in polymer solar cells. J Am Chem Soc 2013;135:1806–15.
[20] Zhou H, Yang L, Stuart AC, Price SC, Liu S, You W. Development of fluorinated benzothiadiazole as a structural unit for a polymer solar cell of 7% efficiency. Angew Chem Int Ed 2011;50:2995–8.
[21] Li Z, Lu J, Tse S, Zhou J, Du X, Tao Y, et al. Synthesis and applications of difluorobenzothiadiazole based conjugated polymers for organic photovoltaics. J Mater Chem 2011;21:3226–33.
[22] Wang N, Chen Z, Wei W, Jiang Z. Fluorinated benzothiadiazole-based conjugated polymers for high-performance polymer solar cells without any processing additives or post-treatments. J Am Chem Soc 2013;135:17060–8.
[23] Chen H, Chen Y, Liu C, Chien Y, Chou S, Chou P. Prominent short-circuit currents of fluorinated quinoxaline-based copolymer solar cells with a power conversion efficiency of 8.0%. Chem Mater 2012;24:4766–72.
[24] Dou L, You J, Yang J, Chen C, He Y, Murase S, et al. Tandem polymer solar cells featuring a spectrally matched low-bandgap polymer. Nat Photonics 2012;6:180–5.
[25] Dou L, Chang W, Gao J, Chen C, You J, Yang Y. A selenium-substituted low-bandgap polymer with versatile photovoltaic applications. Adv Mater 2012;6:825–31.
[26] Ho C, Chen C, Chang C, Darling SB, Su W. Isoindigo-based copolymers for polymer solar cells with efficiency over 7%. J Mater Chem A 2014;2:8026–32.
[27] Guo X, Zhou N, Lou SJ, Smith J, Tice DB, Hennek JW, et al. Polymer solar cells with enhanced fill factors. Nat Photonics 2013;7:825–33.
[28] Nguyen TL, Choi H, Ko SJ, Uddin MA, Walker B, Yum S, et al. Semi-crystalline photovoltaic polymers with efficiency exceeding 9% in a 300 nm thick conventional single-cell device. Energy Environ Sci 2014;7:3040–51.
[29] Chu T, Lu J, Beaupr E S, Zhang Y, Pouliot JEM, Wakim S, et al. Bulk heterojunction solar cells using thieno [3, 4-c] pyrrole-4, 6-dione and dithieno [3, 2-b: 2′, 3′-d] silole copolymer with a power conversion efficiency of 7.3%. J Am Chem Soc 2011;133:4250–3.
[30] Small CE, Tsang S, Chen S, Baek S, Amb CM, Subbiah J, et al. Loss mechanisms in thick-film low-bandgap polymer solar cells. Adv Energy Mater 2013;3:909–16.
[31] Hendriks KH, Heintges GHL, Gevaerts VS, Wienk MM, Janssen RAJ. High-molecular-weight regular alternating diketopyrrolopyrrole-based terpolymers for efficient organic solar cells. Angew Chem Int Ed 2013;52:8341–4.
[32] Kang TE, Kim K, Kim BJ. Design of terpolymers as electron donors for highly efficient polymer solar cells. J Mater Chem A 2014;2:15252–67.
[33] Burkhart B, Khlyabich PP, Thompson BC. Influence of the acceptor composition on physical properties and solar cell performance in semi-random two-acceptor copolymers. ACS Macro Lett 2012;1:660–6.
[34] Jung JW, Liu F, Russell TP, Jo WH. Semi-crystalline random conjugated copolymers with panchromatic absorption for highly efficient polymer solar cells. Energy Environ Sci 2013;6:3301–7.
[35] Chang W, Gao J, Dou L, Chen C, Liu Y, Yang Y. Side-chain tunability via triple component random copolymerization for better photovoltaic polymers. Adv Energy Mater 2013:1300864.
[36] Shen P, Bin H, Xiao L, Li Y. Enhancing photovoltaic performance of copolymers containing thiophene unit with D–A conjugated side chain by rational molecular design. Macromolecules 2013;46:9575–86.
[37] Huang Y, Zhang M, Chen H, Wu F, Cao Z, Zhang L, et al. Efficient polymer solar cells based on terpolymers with a broad absorption range of 300–900 nm. J Mater Chem A 2014;2:5218–23.
[38] Zhang M, Wu F, Cao Z, Shen T, Chen H, Li X, et al. Improved photovoltaic properties of terpolymers containing diketopyrrolopyrrole and an isoindigo side chain. Polym Chem 2014;5:4054–60.
[39] Groves C, Blakesley JC, Greenham NC. Effect of charge trapping on geminate recombination and polymer solar cell performance. Nano Lett 2010;10:1063–9.
[40] Roncali J. Molecular bulk heterojunctions: an emerging approach to organic solar cells. Acc Chem Res 2009;42:1719–30.
[41] Walker B, Kim C, Nguyen T. Small molecule solution-processed bulk heterojunction solar cells. Chem Mater 2011;23:470–82.
[42] Coughlin JE, Henson ZB, Welch GC, Bazan GC. Design and synthesis of molecular donors for solution-processed high-efficiency organic solar cells. Acc Chem Res 2013;47:257–70.
[43] Dou L, You J, Hong Z, Xu Z, Li G, Street RA, et al. 25th Anniversary article: a decade of organic/polymeric photovoltaic research. Adv Mater 2013;25:6642–71.
[44] Zhou J, Wan X, Liu Y, Zuo Y, Li Z, He G, et al. Small molecules based on benzo [1, 2-b: 4, 5-b′] dithiophene unit for high-performance solution-processed organic solar cells. J Am Chem Soc 2012;134:16345–51.
[45] Zhou J, Zuo Y, Wan X, Long G, Zhang Q, Ni W, et al. Solution-processed and high-performance organic solar cells using small molecules with a benzodithiophene unit. J Am Chem Soc 2013;135:8484–7.
[46] Liu Y, Chen C, Hong Z, Gao J, Yang YM, Zhou H, et al. Solution-processed small-molecule solar cells: breaking the 10% power conversion efficiency. Sci Rep 2013;3:3356.
[47] Kan B, Zhang Q, Li M, Wan X, Ni W, Long G, et al. Solution-processed organic solar cells based on dialkylthiol-substituted benzodithiophene unit with efficiency near 10%. J Am Chem Soc 2014;136:15529–32.
[48] van der Poll TS, Love JA, Nguyen T, Bazan GC. Non-basic high-performance molecules for solution-processed organic solar cells. Adv Mater 2012;24:3646–9.
[49] Wang DH, Kyaw AKK, Gupta V, Bazan GC, Heeger AJ. Enhanced efficiency parameters of solution-processable small-molecule solar cells depending on ITO sheet resistance. Adv Energy Mater 2013;3:1161–5.
[50] Qin H, Li L, Guo F, Su S, Peng J, Cao Y, et al. Solution-processed bulk heterojunction solar cells based on a porphyrin small molecule with 7% power conversion efficiency. Energy Environ Sci 2014;7:1397–401.
[51] Hoppe H, Sariciftci NS. Photoresponsive polymers II. Berlin Heidelberg: Springer; 2008. p. 1–86.
[52] Park SH, Roy A, Beaupré S, Cho S, Coates N, Moon JS, et al. Bulk heterojunction solar cells with internal quantum efficiency approaching 100%. Nat Photonics 2009;3:297–302.
[53] Liang Y, Xu Z, Xia J, Tsai S, Wu Y, Li G, et al. For the bright future—bulk heterojunction polymer solar cells with power conversion efficiency of 7.4%. Adv Mater 2010;22:135–8.
[54] Zou Y, Najari A, Berrouard P, Beaupré S, Réda Aïch B, Tao Y, et al. A thieno [3,4-c]pyrrole-4,6-dione-based copolymer for efficient solar cells. J Am Chem Soc 2010;132:5330–1.
[55] Brabec CJ, Cravino A, Meissner D, Sariciftci NS, Fromherz T, Rispens MT, et al. Origin of the open circuit voltage of plastic solar cells. Adv Funct Mater 2001;11:374–80.
[56] Hummelen JC, Knight BW, LePeq F, Wudl F, Yao J, Wilkins CL. Preparation and characterization of fulleroid and methanofullerene derivatives. J Org Chem 1995;60:532–8.
[57] Wienk MM, Kroon JM, Verhees WJH, Knol J, Hummelen JC, van Hal PA, et al. Efficient methano[70]fullerene/MDMO-PPV bulk heterojunction photovoltaic cells. Angew Chem Int Ed 2003;42:3371–5.
[58] He Y, Chen H, Hou J, Li Y. Indene−C60 bisadduct: a new acceptor for high-performance polymer solar cells. J Am Chem Soc 2010;132:1377–82.
[59] Griffini G, Douglas JD, Piliego C, Holcombe TW, Turri S, Fréchet JMJ, et al. Long-term thermal stability of high-efficiency polymer solar cells based on photocrosslinkable donor-acceptor conjugated polymers. Adv Mater 2011;23:1660–4.
[60] Williams G, Wang Q, Aziz H. The photo-stability of polymer solar cells: contact photo-degradation and the benefits of interfacial layers. Adv Funct Mater 2013;23:2239–47.
[61] Hermenau M, Riede M, Leo K, Gevorgyan SA, Krebs FC, Norrman K. Water and oxygen induced degradation of small molecule organic solar cells. Sol Energy Mater Sol Cells 2011;95:1268–77.
[62] Grossiord N, Kroon JM, Andriessen R, Blom PWM. Degradation mechanisms in organic photovoltaic devices. Org Electron 2012;13:432–56.
[63] Bertho S, Janssen G, Cleij TJ, Conings B, Moons W, Gadisa A, et al. Effect of temperature on the morphological and photovoltaic stability of bulk heterojunction polymer:fullerene solar cells. Sol Energy Mater Sol Cells 2008;92:753–760.
[64] Tromholt T, Manor A, Katz EA, Krebs FC. Reversible degradation of inverted organic solar cells by concentrated sunlight. Nanotechnology 2011;22:225401.
[65] Gevorgyan SA, Jørgensen M, Krebs FC, Sylvester-Hvid KO. A compact multi-chamber setup for degradation and lifetime studies of organic solar cells. Sol Energy Mater Sol Cells 2011;95:1389–97.
[66] Jørgensen M, Norrman K, Gevorgyan SA, Tromholt T, Andreasen B, Krebs FC. Stability of polymer solar cells. Adv Mater 2012;24:580–612.
[67] Jørgensen M, Norrman K, Krebs FC. Stability/degradation of polymer solar cells. Sol Energy Mater Sol Cells 2008;92:686–714.
[68] Schüth F. Encapsulation strategies in energy conversion materials. Chem Mater 2014;26:423–34.
[69] Tanenbaum DM, Dam HF, Rösch R, Jørgensen M, Hoppe H, Krebs FC. Edge sealing for low cost stability enhancement of roll-to-roll processed flexible polymer solar cell modules. Sol Energy Mater Sol Cells 2012;97:157–63.

[70] Wang F, Tan Z, Li Y. Solution-processable metal oxides/chelates as electrode buffer layers for efficient and stable polymer solar cells. Energy Environ Sci 2015;8:1059–91.
[71] Rumer JW, Ashraf RS, Eisenmenger ND, Huang Z, Meager I, Nielsen CB, et al. Dual function additives: a small molecule crosslinker for enhanced efficiency and stability in organic solar cells. Adv Energy Mater 2015;5:1401426.
[72] Kesters J, Verstappen P, Raymakers J, Vanormelingen W, Drijkoningen J, D Haen J, et al. Enhanced organic solar cell stability by polymer (PCPDTBT) side chain functionalization. Chem Mater 2015;27:1332–41.
[73] Li Y, You Y, Zhou H. Beijing: Chemical Industry Press; 2013. p. 66–113.
[74] de Jong MP, van IJzendoorn LJ, de Voigt MJA. Stability of the interface between indium-tin-oxide and poly(3,4-ethylenedioxythiophene)/poly(styrenesulfonate) in polymer light-emitting diodes. Appl Phys Lett 2000;77:2255–7.
[75] Irwin MD, Buchholz DB, Hains AW, Chang RPH, Marks TJ. p-Type semiconducting nickel oxide as an efficiency-enhancing anode interfacial layer in polymer bulk-heterojunction solar cells. Proc Natl Acad Sci USA 2008;105:2783–7.
[76] Shrotriya V, Li G, Yao Y, Chu C, Yang Y. Transition metal oxides as the buffer layer for polymer photovoltaic cells. Appl Phys Lett 2006;88:73508.
[77] Ndione PF, Garcia A, Widjonarko NE, Sigdel AK, Steirer KX, Olson DC, et al. Highly-tunable nickel cobalt oxide as a low-temperature p-type contact in organic photovoltaic devices. Adv Energy Mater 2013;3:524–31.
[78] Tan ZA, Li L, Cui C, Ding Y, Xu Q, Li S, et al. Solution-processed tungsten oxide as an effective anode buffer layer for high-performance polymer solar cells. J Phys Chem C 2012;116:18626–32.
[79] Tan Z, Qian D, Zhang W, Li L, Ding Y, Xu Q, et al. Efficient and stable polymer solar cells with solution-processed molybdenum oxide interfacial layer. J Mater Chem A 2013;1:657–64.
[80] Sun Y, Takacs CJ, Cowan SR, Seo JH, Gong X, Roy A, et al. Efficient, air-stable bulk heterojunction polymer solar cells using MoO_x as the anode interfacial layer. Adv Mater 2011;23:2226–30.
[81] Murase S, Yang Y. Solution processed MoO_3 interfacial layer for organic photovoltaics prepared by a facile synthesis method. Adv Mater 2012;24:2459–62.
[82] Tan Z, Zhang W, Cui C, Ding Y, Qian D, Xu Q, et al. Solution-processed vanadium oxide as a hole collection layer on an ITO electrode for high-performance polymer solar cells. Phys Chem Chem Phys 2012;14:14589–95.
[83] Tan Z, Li L, Wang F, Xu Q, Li S, Sun G, et al. Solution-processed rhenium oxide: a versatile anode buffer layer for high performance polymer solar cells with enhanced light harvest. Adv Energy Mater 2014;4:1300884.
[84] Zhou H, Zhang Y, Mai C, Collins SD, Nguyen T, Bazan GC, et al. Conductive conjugated polyelectrolyte as hole-transporting layer for organic bulk heterojunction solar cells. Adv Mater 2014;26:780–5.
[85] Uyeda N, Kobayashi T, Ishizuka K, Fujiyoshi Y. Crystal structure of Ag TCNQ. Nature 1980;285:95–7.
[86] Ishii H, Sugiyama K, Ito E, Seki K. Energy level alignment and interfacial electronic structures at organic/metal and organic/organic interfaces. Adv Mater 1999;11:605–25.
[87] Fujishima A, Honda K. Electrochemical photolysis of water at a semiconductor electrode. Nature 1972;238:37–8.
[88] O'Regan B, Gratzel M. A low-cost, high-efficiency solar cell based on dye-sensitized colloidal TiO_2 films. Nature 1991;353:737–40.
[89] Fujishima A, Rao TN, Tryk DA. Titanium dioxide photocatalysis. J Photochem Photobiol C 2000;1:1–21.
[90] Linsebigler AL, Lu G, Yates JT. Photocatalysis on TiO_2 surfaces: principles, mechanisms, and selected results. Chem Rev 1995;95:735–58.
[91] Lee K, Kim JY, Park SH, Kim SH, Cho S, Heeger AJ. Air-stable polymer electronic devices. Adv Mater 2007;19:2445–9.
[92] Kawano K, Pacios R, Poplavskyy D, Nelson J, Bradley DDC, Durrant JR. Degradation of organic solar cells due to air exposure. Sol Energy Mater Sol Cells 2006;90:3520–30.
[93] Yan H, Lee P, Armstrong NR, Graham A, Evmenenko GA, Dutta P, et al. High-performance hole-transport layers for polymer light-emitting diodes. Implementation of organosiloxane cross-linking chemistry in polymeric electroluminescent devices. J Am Chem Soc 2005;127:3172–83.
[94] Norrman K, Gevorgyan SA, Krebs FC. Water-induced degradation of polymer solar cells studied by $H_2^{18}O$ labeling. ACS Appl Mater Interfaces 2009;1:102–12.
[95] Waldauf C, Morana M, Denk P, Schilinsky P, Coakley K, Choulis SA, et al. Highly efficient inverted organic photovoltaics using solution based titanium oxide as electron selective contact. Appl Phys Lett 2006;89:233517.
[96] White MS, Olson DC, Shaheen SE, Kopidakis N, Ginley DS. Inverted bulk-heterojunction organic photovoltaic device using a solution-derived ZnO underlayer. Appl Phys Lett 2006;89:143517.
[97] Li G, Chu CW, Shrotriya V, Huang J, Yang Y. Efficient inverted polymer solar cells. Appl Phys Lett 2006;88:253503.
[98] Krebs FC. Polymer solar cell modules prepared using roll-to-roll methods: knife-over-edge coating, slot-die coating and screen printing. Sol Energy Mater Sol Cells 2009;93:465–75.
[99] Chen J, Cui C, Li Y, Zhou L, Ou Q, Li C, et al. Single-junction polymer solar cells exceeding 10% power conversion efficiency. Adv Mater 2015;27:1035–41.
[100] Liao S, Jhuo H, Cheng Y, Chen S. Fullerene derivative-doped zinc oxide nanofilm as the cathode of inverted polymer solar cells with low-bandgap polymer (PTB7-Th) for high performance. Adv Mater 2013;25:4766–71.
[101] Small CE, Chen S, Subbiah J, Amb CM, Tsang S, Lai T, et al. High-efficiency inverted dithienogermole–thienopyrrolodione-based polymer solar cells. Nat Photonics 2011;6:115–20.
[102] Chen S, Small CE, Amb CM, Subbiah J, Lai T, Tsang S, et al. Inverted polymer solar cells with reduced interface recombination. Adv Energy Mater 2012;2:1333–7.
[103] Adhikary P, Venkatesan S, Adhikari N, Maharjan PP, Adebanjo O, Chen J, et al. Enhanced charge transport and photovoltaic performance of PBDTTT-C-T/PC70BM solar cells via UV–ozone treatment. Nanoscale 2013;5:10007–13.
[104] He Z, Zhong C, Su S, Xu M, Wu H, Cao Y. Enhanced power-conversion efficiency in polymer solar cells using an inverted device structure. Nat Photonics 2012;6:593–7.
[105] Yang T, Wang M, Duan C, Hu X, Huang L, Peng J, et al. Inverted polymer solar cells with 8.4% efficiency by conjugated polyelectrolyte. Energy Environ Sci 2012;5:8208–14.
[106] Tan Z, Zhang W, Zhang Z, Qian D, Huang Y, Hou J, et al. High-performance inverted polymer solar cells with solution-processed titanium chelate as electron-collecting layer on ITO electrode. Adv Mater 2012;24:1476–81.
[107] Deng Y, Liu J, Wang J, Liu L, Li W, Tian H, et al. Dithienocarbazole and isoindigo based amorphous low bandgap conjugated polymers for efficient polymer solar cells. Adv Mater 2013;3:471–6.
[108] Liao S, Jhuo H, Yeh P, Cheng Y, Li Y, Lee Y, et al. Single junction inverted polymer solar cell reaching power conversion efficiency 10.31% by employing dual-doped zinc oxide nano-film as cathode interlayer. Sci Rep 2014;4:6813.
[109] Nielsen CB, Ashraf RS, Treat ND, Schroeder BC, Donaghey JE, White AJP, et al. 2,1,3-Benzothiadiazole-5,6-dicarboxylic imide – a versatile building block for additive- and annealing-free processing of organic solar cells with efficiencies exceeding 8%. Adv Mater 2015;27:948–53.
[110] Zhang Z, Lin F, Chen H, Wu H, Chung C, Lu C, et al. A silole copolymer containing a ladder-type heptacylic arene and naphthobisoxadiazole moieties for highly efficient polymer solar cells. Energy Environ Sci 2015;8:552–7.
[111] Scharber MC, Mühlbacher D, Koppe M, Denk P, Waldauf C, Heeger AJ, et al. Design rules for donors in bulk-heterojunction solar cells—towards 10% energy-conversion efficiency. Adv Mater 2006;18:789–94.
[112] Koster LJA, Mihailetchi VD. Blom PWM. Ultimate efficiency of polymer/fullerene bulk heterojunction solar cells. Appl Phys Lett 2006;88:93511.
[113] Scharber MC, Sariciftci NS. Efficiency of bulk-heterojunction organic solar cells. Prog Polym Sci 2013;38:1929–40.
[114] Kim JY, Lee K, Coates NE, Moses D, Nguyen T, Dante M, et al. Efficient tandem polymer solar cells fabricated by all-solution processing. Science 2007;317:222–5.
[115] Ameri T, Dennler G, Lungenschmied C, Brabec CJ. Organic tandem solar cells: a review. Energy Environ Sci 2009;2:347–63.
[116] Sista S, Hong Z, Park M, Xu Z, Yang Y. High-efficiency polymer tandem solar cells with three-terminal structure. Adv Mater 2010;22:E77–80.
[117] Sista S, Hong Z, Chen L, Yang Y. Tandem polymer photovoltaic cells-current status, challenges and future outlook. Energy Environ Sci 2011;4:1606–20.
[118] Gevaerts VS, Furlan A, Wienk MM, Turbiez M, Janssen RAJ. Solution processed polymer tandem solar cell using efficient small and wide bandgap polymer: fullerene blends. Adv Mater 2012;24:2130–4.
[119] Li N, Baran D, Spyropoulos GD, Zhang H, Berny S, Turbiez M, et al. Environmentally printing efficient organic tandem solar cells with high fill factors: a guideline towards 20% power conversion efficiency. Adv Energy Mater 2014;4:1400084.
[120] Etxebarria I, Ajuria J, Pacios R. Solution-processable polymeric solar cells: a review on materials, strategies and cell architectures to overcome 10%. Org Electron 2015;19:34–60.
[121] You J, Chen C, Hong Z, Yoshimura K, Ohya K, Xu R, et al. 10.2% power conversion efficiency polymer tandem solar cells consisting of two identical sub-cells. Adv Mater 2013;25:3973–8.
[122] You J, Dou L, Yoshimura K, Kato T, Ohya K, Moriarty T, et al. A polymer tandem solar cell with 10.6% power conversion efficiency. Nat Commun 2013;4:1446.
[123] Li K, Li Z, Feng K, Xu X, Wang L, Peng Q. Development of large band-gap conjugated copolymers for efficient regular single and tandem organic solar cells. J Am Chem Soc 2013;135:13549–57.
[124] Chang C, Zuo L, Yip H, Li Y, Li C, Hsu C, et al. A versatile fluoro-containing low-bandgap polymer for efficient semitransparent and tandem polymer solar cells. Adv Funct Mater 2013;23:5084–90.
[125] Zhou H, Zhang Y, Mai C, Collins SD, Bazan GC, Nguyen T, et al. Polymer homo-tandem solar cells with best efficiency of 11.3%. Adv Mater 2015;27:1767–73.
[126] Li W, Furlan A, Hendriks KH, Wienk MM, Janssen RAJ. Efficient tandem and triple-junction polymer solar cells. J Am Chem Soc 2013;135:5529–32.
[127] Che X, Xiao X, Zimmerman JD, Fan D, Forrest SR. High-efficiency, vacuum-deposited, small-molecule organic tandem and triple-junction photovoltaic cells. Adv Energy Mater 2014;4:1400568.
[128] Chen C, Chang W, Yoshimura K, Ohya K, You J, Gao J, et al. An efficient triple-junction polymer solar cell having a power conversion efficiency exceeding 11%. Adv Mater 2014;26:5670–7.
[129] Yusoff ARBM, Kim D, Kim HP, Shneider FK, Da Silva WJ, Jang J. A high efficiency solution processed polymer inverted triple-junction solar cell exhibiting a power conversion efficiency of 11.83%. Energy Environ Sci 2015;8:303–16.
[130] Mazzio KA, Luscombe CK. The future of organic photovoltaics. Chem Soc Rev 2015;44:78–90.